

NASA
Technical Memorandum 87091

USAAVSCOM
Technical Report 85-C-12

Three-Dimensional Inviscid Analysis of Radial Turbine Flow and a Limited Comparison With Experimental Data

(NASA-TM-87091) THREE-DIMENSIONAL INVISCID ANALYSIS OF RADIAL TURBINE FLOW AND A LIMITED COMPARISON WITH EXPERIMENTAL DATA (NASA) 28 p HC A03/MF A01 C SCL 01A N86-10017 Unclas G3/02 27501

Y.K. Choo
Lewis Research Center
Cleveland, Ohio

and

K.C. Civinskas
Propulsion Directorate
U.S. Army Aviation Research and Technology Activity (AVSCOM)
Lewis Research Center
Cleveland, Ohio

Prepared for the
Three-Dimensional Flow Phenomena in Fluid Machinery Symposium
ASME Winter Annual Meeting
Miami, Florida, November 17-22, 1985

NASA



THREE-DIMENSIONAL INVISCID ANALYSIS OF RADIAL TURBINE FLOW AND A LIMITED
COMPARISON WITH EXPERIMENTAL DATA

Y.K. Choo
National Aeronautics and Space Administration
Lewis Research Center
Cleveland, Ohio 44135

and

K.C. Civinskas
Propulsion Directorate
U.S. Army Aviation Research and Technology Activity (AVSCOM)
Lewis Research Center
Cleveland, Ohio 44135

SUMMARY

The three-dimensional inviscid DENTON code was used to analyze flow through a radial-inflow turbine rotor. Experimental data from the rotor are compared with analytical results obtained by using the code. The experimental data available for comparison are the radial distributions of circumferentially averaged values of absolute flow angle and total pressure downstream of the rotor exit. The computed rotor-exit flow angles are generally underturned relative to the experimental values, which reflect the boundary-layer separation at the trailing edge and the development of wakes downstream of the rotor. The experimental rotor was designed for a higher-than-optimum work factor of 1.126 resulting in a nonoptimum positive incidence and causing a region of rapid flow adjustment and large velocity gradients. For this experimental rotor, the computed radial distribution of rotor-exit to turbine-inlet total pressure ratios are underpredicted due to the errors in the finite-difference approximations in the regions of rapid flow adjustment and due to using the relatively coarser grids in the middle of the blade region where the flow passage is highly three-dimensional. Additional results obtained from the three-dimensional inviscid computation are also presented, but without comparison due to the lack of experimental data. These include quasi-secondary velocity vectors on cross-channel surfaces, velocity components on the meridional and blade-to-blade surfaces, and blade surface loading diagrams. Computed results show the evolution of a passage vortex and large streamline deviations from the computational streamwise grid lines. Experience gained from applying the code to a radial turbine geometry is also discussed.

INTRODUCTION

The radial-inflow turbine continues to be a candidate configuration for many small size applications ranging from ground transportation to space power. The rotor passages are highly three-dimensional and have low aspect ratios compared with axial turbines. Typical geometries, which turn flow through 90° of deflection in the meridional plane while simultaneously turning the flow in the blade-to-blade plane naturally induce large three-dimensional secondary flows even in the absence of viscous effects. Even though quasi-three-dimensional techniques can provide valuable guidance for design analysis of

such geometries, as was done in reference 1, it is clear that these geometries should benefit further from fully three-dimensional approaches. While the effects of viscosity should ultimately be included, the results obtained from a solution of the Euler equations are useful in preliminary design work where information on pressure alone is desired. In problems where heat transfer and skin friction are required, a solution of the boundary-layer equations provides an adequate approximation. But, the outer-edge boundary conditions, including pressure, must be established from the inviscid solution as the first step in such an analysis (ref. 2). A parabolized Navier-Stokes solver (ref. 3), for instance, uses an inviscid pressure field as an initial pressure field.

Development of a fully three-dimensional inviscid code for turbomachinery flows was reported by Denton (ref. 4), and this code was used for solutions of the Euler equations through blade rows (ref. 5). The method was later improved through the simple nonoverlapping grid and multigrid solution scheme described in references 6 and 7. The version of the code reported in reference 6 was assessed in reference 8 by comparing computed results with experimental data from an axial annular cascade (ref. 9) and from an axial turbine stage (ref. 10). Reported flow angles and velocity components obtained from the inviscid computation by the DENTON code and experiment were in good agreement with the annular cascade data. The DENTON code also gave reasonable agreement for the temperature distribution at the exit of a low-aspect-ratio axial turbine rotor with a nonuniform temperature distribution imposed at the inlet. The code, however, gave substantially different rotor-exit flow-angle distributions.

An objective of the current effort was to extend the assessment of the DENTON code to a radial turbine configuration. The code was used to analyze the flow through the radial-inflow turbine rotor described in reference 11 and to compare computed results with experimental data. The rotor blades of this 15.04-cm-diameter radial turbine were designed thick to allow for internal cooling passages and trailing-edge coolant ejection. The test rotor, however, was a solid rotor with no coolant flows involved. Since the experimental program was undertaken primarily to determine overall performance, no detailed measurements internal to the rotor passage were made, and the available experimental data are limited to rotor-inlet and -exit surveys. The radial distribution of absolute flow angle and total pressure from the experiment are compared with the computed results. Other computed results are presented in the form of velocity-vector plots, loading diagrams, and contour plots. Most computed results are presented without comparison because of the lack of experimental data. Some of the flow characteristics are qualitatively compared with analytical results of Bosman and Highton (ref. 12) as well as a quasi-three-dimensional analysis.

EXPERIMENTAL DATA

Experimental data from a 15.04-cm-tip-diameter radial-inflow turbine rotor were obtained from reference 11. The actual rotor used in the experiment is shown in figure 1. The rotor had 12 full blades that were thick enough to allow internal cooling passages and the trailing-edge ejection of coolant. For the turbine tests reported in the reference, however, the blading was solid with no coolant ejection. The rotor had unswept radial blades at the inducer inlet and large blockages (78.7, 38.2, and 14.9 percent at the hub, mean, and tip, respectively) resulting from the thick trailing edges. The test program

described in reference 11 was undertaken primarily to obtain overall performance and an internal loss breakdown. No detailed flow measurements within the rotor blading itself were obtained, but the results of rotor inlet and exit surveys reported for one operating condition are the basis for this limited comparison with the DENTON code.

A rotor-inlet survey of absolute flow angle and absolute total pressure was made just upstream of the rotor leading edge (station 3 of ref. 11). The surveys were made over 2 stator vane passages and at 11 axial positions from hub to shroud. For each axial position, data were taken at 11 circumferential positions and arithmetically averaged. Figure 2 shows the distribution of rotor-inlet flow angles and the mass-averaged absolute flow angle of 73.6° from the experiment. The flow angles at the hub and shroud walls shown in the distribution are those required to match continuity.

Similarly, a rotor-exit survey was taken about 2.8 cm downstream of the rotor trailing edge (station 4 of ref. 11). These data were taken at 11 radial locations, all at one circumferential position. The radial distribution of absolute flow angle and total pressure ratio, measured at this location, are presented in figure 3.

A summary of the overall rotor conditions is given in table I. Even though mass flow is not an input to the DENTON code, it is given for comparison purposes later. The experimental conditions used as inputs to the inviscid code were for corrected design speed, temperature, and pressure ratio. The rotor-inlet total pressure reflects the 6.3-percent measured loss due to the stator and vaneless space.

INVISCID COMPUTATION

The three-dimensional inviscid DENTON code was used to analyze the radial rotor. The stator was not included in this analysis. The code, developed by Denton, uses an explicit time marching method for turbomachinery flow calculation. The code solves the Euler equations in finite-volume form using an opposed-difference scheme in which changes in the fluxes of mass, momentum, and energy move downwind and pressure moves upwind. A two-level multigrid feature of the code was used to reduce computation time, and variable time steps were also used to reduce computation time while maintaining stability.

The computational mesh for two blade-to-blade surfaces and on the meridional plane are shown in figures 4 and 5, respectively. The number of grid lines used are 13 in the blade-to-blade direction ($I = 1$ on the suction surface, $I = 13$ on the pressure surface), 73 in the stream-wise direction ($J = 1$ at upstream boundary, $J = 73$ at downstream boundary), and 21 in the hub-to-shroud direction ($K = 1$ on the hub surface and $K = 21$ on the tip). As indicated in figure 5, the leading edge is at $J = 12$, the trailing edge at $J = 60$, station 3 at about $J = 9$, and station 4 at $J = 73$. Nonuniform grid spacing was used in all three directions. The packing of quasi-orthogonal mesh lines was used to get higher resolutions near the leading and trailing edges. In addition, this feature was used to position the initial upstream grid at any desired location with a selected number of orthogonal grid lines, and to position the final downstream grid where the experimental data were measured so that the Denton outputs could be directly compared with the experimental results at station 4.

The leading-edge region was of particular concern in this effort. Unlike an axial turbine which has a slightly negative optimum incidence, a 12-bladed radial rotor achieves optimum incidence at a much higher negative incidence (at -36.7° relative inlet flow angle for this design). This implies a region of very rapid flow adjustment and large velocity gradients in the leading-edge region of a radial turbine. The blade loadings reach their maxima in this region where the incoming negatively incident streamlines are turned toward zero incidence at the rotor inducer tip. The varying radius in this region also contributes to the rapidly varying flow field. To complicate matters further, the subject rotor was designed for a higher-than-optimum work factor of 1.126 resulting in a nonoptimum positive incidence of 16.5° . An optimum work factor for this rotor is 0.833 (ref. 11). Besides the grid packing near the leading edge, cusps were extended in this region to eliminate singularity and to minimize discontinuities in the grid slope. The cusps carry no load, and, therefore, periodicity is automatically satisfied. Figure 6 shows two types of leading-edge cusps that were used. In the blunt leading edge on the left, the cusps were extended over three grid spaces. In the rounded leading edge on the right, the cusps were extended over one grid space. This rounded leading-edge geometry more closely approximates the circular leading edge of the real hardware. It should be noted that Denton presents results for a radial turbine geometry in reference 7. The blade geometry shown there, however, differs substantially from the rotor considered here. Denton's geometry shows a more rounded leading edge (resembling an axial turbine blade) rather than a typical highly stressed radial turbine blade.

Since the blades were originally designed to have internal cooling passages, they are exceptionally thick, which results in the large blockage at the trailing edge as indicated in the previous section. The use of cusps at the trailing edges was necessary to get convergent solutions. The cusp at the trailing edge needed to be extended over six grid spaces.

As mentioned earlier, the input data obtained from reference 11 to run the code included the blade geometry, absolute flow angle at the rotor inlet shown in figure 3, total pressure and temperature at the rotor inlet, the hub static pressure at the rotor exit, and rotational speed (table I). The actual input dataset for the DENTON code was generated by using an input generator code (ref. 13).

A user of the DENTON code has an option to specify absolute swirl angle at the inlet and to allow swirl velocity to vary. This option was used, since inlet absolute swirl angle data were available from the experiment (ref. 11). With this option and the computational grids shown in figures 4 and 5, the authors had no problem in getting convergent solutions. Convergence was taken to occur when the average change in meridional velocity per cycle was less than the value of 2×10^{-6} times an average velocity for the whole flow. Smaller time increments (time multiplier value of approximately 0.1) were required because of the fine grid spacings used. Both the average constant value and the measured profile of the absolute swirl angle shown in figure 2 were tried. Since computed results of both cases at station 4 were about the same, only the results based on the average absolute flow angle of 73.6° are now presented.

Convergence of an initial computation was obtained using a computational domain which extended between two data monitoring stations of the experimental work (i.e., between station 3 and 4 shown in fig. 5). It should be pointed

out that station 3 is very close to the leading edge of the rotor blade and station 4 is 2.8 cm downstream from the trailing edge. In this case, even though the velocity field converged, examination of results indicated that the results were not correct. Because the upstream boundary was very close to the leading edge and the rotor-inlet absolute flow angle at station 3 was specified and fixed, both flow direction and velocity rapidly changed around the leading edge, especially on the suction side. This rapid change in direction and magnitude evidently caused errors in the finite-difference approximations, which are manifested as stagnation pressure changes in the flow. When this situation is expected, users should check the ratios of the computed pressure to ideal pressure obtained from an isentropic process. These computed to ideal pressure ratios at all grid points are available as a part of output. If these pressure ratios are far from unity, close scrutiny of results is needed. Further discussions on the entropy and total pressure changes in the time marching scheme can be found in reference 6.

Three actions were taken to correct the situation. First, the pitchwise spacing of grid lines was packed near the blade surfaces in addition to the streamwise grid packing around the leading and trailing edges, following the suggestions made by Denton and Singh in reference 5. Second, the upstream region of the computational domain was extended beyond station 3 by using a larger number of grids and variable streamwise spacing. Third, cusps were used at the leading and trailing edges to reduce the changes in entropy and total pressure due to the errors in finite-differencing scheme around these regions. The results presented in this paper were obtained with these changes.

RESULTS

Flow Angle

Figure 7 shows the calculated absolute flow angle distribution on the cross-channel surface at station 4. To compare with experimental data, these flow angles were circumferentially mass averaged at each grid location between hub and shroud. The radial distribution of these averaged absolute flow angles are then compared with the experimental data in figure 8.

Figure 8(a) shows a comparison of the computed rotor exit flow angles with the experimental data. Two computed cases are those with the blunt and rounded leading edges shown in figure 6. Both cases used cusps at the trailing edges and the experimental operating conditions presented in table I. The computed rotor-exit flow angles are underturned relative to the experimental data, particularly near the hub. This large deviation of the computed flow angles near the hub from the experimental data could be anticipated. In the actual experiment, a flow separation off the trailing edge and a development of strong wakes could be anticipated due to the large trailing-edge blockage (78.7 percent at the hub). Obviously, these effects are not included in the inviscid analysis, and the flow is diffused without separation in the calculation. The case with rounded leading edges shows a flatter distribution than the result of the blunt leading-edge case.

Figure 8(b) shows the effect of 2° reduction in the rotor-inlet absolute flow angle towards optimum incident angle of this rotor design. This is shown using the blunt leading-edge case. With the reduced inlet flow angle the rotor-exit flow angles are overturned relative to the experimental values in

the outer portion of the exit annulus and underturned near the hub. Results of the DENTON code for this reduced inlet angle case indicate that the 2° reduction reduces total pressure changes by noticeable amounts.

Total Pressure Ratio

Calculated total pressure distribution on the cross-channel surface at station 4 is shown in figure 9. To compare with experimental data, the rotor-exit to turbine-inlet total pressure ratios on this cross-channel surface are circumferentially mass averaged at each grid location between hub and shroud. The radial distributions of the pressure ratios are compared in figure 10.

Figure 10(a) compares the computed results with the experimental data. The computed case is again the one that uses the experimental operating condition, cusps at the leading and trailing edges, and the mass-averaged experimental value of 73.6° absolute flow angle at the rotor inlet. The overall level of the total pressure at station 4 remains at about the same level for the two computed cases with the blunt and rounded leading edges. And, except in a small region near the hub, the calculated pressure ratios are underpredicted relative to the experimental data. In spite of the efforts made to reduce the numerical losses by using fine grids near the leading and trailing edges, by using cusps, and by extending the upstream computational domain beyond the rotor-inlet survey location (station 3), it appears that the overall effect of the entropy change on the total pressure is more than the effect of actual viscosity on the total pressure in the experimental flow. For this experimental rotor blade, which was designed thick to incorporate internal cooling and designed for a higher than optimum work factor, entropy changes due to the finite-difference errors result in large total pressure losses. Large entropy and total pressure changes resulted around the leading edges, particularly on the suction side. Because of the large blockage from the thick trailing edge, especially at the hub (78.7 percent), the use of even finer grid spacings near the leading and trailing edges only requires unnecessarily finer time steps without further reducing the numerical errors. No further effort was made to modify the code to increase the currently available number of grid spaces for the cusp at the leading edge. Compared with the ideal total pressures between the rotor inlet and exit, the calculated total pressures for the blunt leading-edge case show about 6-percent error at $K = 1$ (at the hub), 5-percent error at $K = 6$, 7-percent error at $K = 11$ (midspan), 10-percent error at $K = 16$, and 12-percent at $K = 21$ (tip).

Figure 10(b) shows the effect of reducing the rotor-inlet absolute flow angle toward the optimum incidence angle by 2°. The effect is shown using the blunt leading-edge case. The reduction results in a reduction of total pressure losses. Compared with the ideal total pressures, the calculated total pressures for the reduced inlet flow angle show about 7-percent error at the hub, 4-percent at the midspan, and 9-percent at the tip. With this reduction, the calculated total pressures are at about the same level as the viscous experimental flow.

Mass Flow

For the same rotor operating conditions used in the experiment (table I), it was anticipated that the mass flow rate calculated by the inviscid code

would be higher than the experimental mass flow rate. But, the rate estimated by the DENTON code (0.2352 kg/s for the blunt leading-edge case and 0.239 kg/s for the rounded leading-edge case) is very close to the experimental value of 0.2372 kg/s due to the total pressure losses discussed earlier. The case with the reduced rotor inlet flow angle has an increased mass flow rate of 0.2646 kg/s because it produces less total pressure losses.

Velocities

Figure 11 shows quasi-secondary velocity vectors on cross-channel surfaces. The primary flow direction is chosen arbitrarily to be the streamwise grid direction in determining the secondary flow vectors. The velocity vectors shown in the figure are the projections of these secondary velocity vectors on the cross-channel surfaces constructed for the computation. Computed results indicate that the average magnitude of the quasi-secondary flow vectors on the cross-channel surfaces is about 17 percent of the average meridional velocity in the blade region. A fraction of the average meridional velocity is indicated in the figure to show the relative strength of secondary flow in the rotor flow passage. As shown in the figure, the secondary flow in the first half of the blade passage is mostly in the direction from the suction surface to the pressure surface. But, in the middle of the passage at $J = 39$ where the flow passage begins to turn in the tangential direction in addition to the continuous turn in the meridional plane, a weak single passage vortex is developed and its strength is increased for the remaining blade passage. The evolution of the passage vortex is attributable to the highly three-dimensional rotor passage and rotation of the blade.

Velocity components projected on the meridional surfaces are presented in figure 12. It can be observed from the figure that fluid entering the blade region on the suction surface migrates towards the shroud, while that entering on the pressure surface migrates towards the hub. Similar results are reported by Bosman and Highton (ref. 12). For comparison, figure 13(a) shows the meridional streamlines predicted by a quasi-three-dimensional analysis (ref. 14), figure 13(b) shows the streamlines on the suction surface predicted by the DENTON code, and figure 13(c) shows the streamlines on the pressure surface predicted by the DENTON code. The large deviations in flow angle between the fully three-dimensional and quasi-three-dimensional analyses are evident, especially in the exducer region.

Velocity vectors are plotted on blade-to-blade surfaces in figure 14. Streamlines predicted on the hub and tip surfaces are shown in figure 15. It can be observed that fluid entering the blade at midpitch on the hub migrates towards to the pressure surface in the first half of the blade passage, but, in the latter half of the passage, it remigrates back toward the suction surface. Fluid entering the blade at midpitch on the shroud section migrates toward the pressure surface throughout the entire blade passage. This result qualitatively agrees with the result of Bosman and Highton (ref. 12).

A contour plot of the relative critical velocity ratio on a midspan blade to blade surface is presented in figure 16. The critical velocity ratio is the ratio of fluid velocity to critical velocity, which is equal to the velocity of sound at the critical condition. It shows a rapid change in the critical velocity ratio around the leading edge on the suction side. A small region of sonic flow appears on the suction side leading edge with a peak

velocity ratio of 1.14. The blunt leading-edge case produced a peak velocity ratio of about 1.32 in the same region.

Blade Surface Loadings

Loading diagrams for the radial rotor blade at the hub, midspan, and tip are presented in figure 17. It is shown that most loading is exerted in the forward half of the blade. For the latter half of the blade where the flow is mostly in the axial direction, a small adverse loading occurs at the hub, and disappears by midspan. No Kutta condition is enforced by the DENTON code and the loading diagram at the tip section is slightly open at the trailing edge.

CONCLUDING REMARKS

Application of the DENTON code has been made to an experimental radial-inflow turbine rotor. The rotor had 12 full blades thick enough to allow internal cooling passages and the trailing-edge ejection of coolant. It had unswept radial blades at the inducer inlet and large blockages resulting from the thick trailing edges. The rotor was also designed for a higher-than-optimum work factor resulting in a large, nonoptimum positive incidence. For this rotor, the fully three-dimensional DENTON code predicted an evolution of a passage vortex. Computed results also show highly twisted streamlines suggesting that the quasi-three-dimensional analysis might not be valid for the flow through this radial turbine rotor passage. To get the solutions reported herein, it was necessary to use fine grid lines near the leading and trailing edges, to use cusps at the leading and trailing edges, and to extend the upstream computational domain beyond the rotor-inlet survey station of the experiment, which was very close to the leading edge.

Since detailed flow measurements within the rotor blading itself are not available, the comparison of the computed results with the experimental data is limited to the data at rotor exit. The computed rotor-exit flow angles are generally underturned relative to the experimental values, especially near the hub region where the blockage at the trailing edge is very large. The computed radial distribution of the rotor-exit to turbine-inlet total pressure ratios are underpredicted for this exceptionally thick, highly loaded experimental rotor blade because of the errors in the finite-difference approximations in the regions of the rapid flow adjustment and because of using the relatively coarser grids in the middle of the blade region where the flow passage is highly three-dimensional.

Even with this extremely difficult geometry and flow field, the DENTON code predicted flow angles fairly well where trailing-edge blockage was not excessive. Certainly, it must be used judiciously for such radial geometries. Additional experimental data are needed for more definitive assessment of the code.

REFERENCES

1. Civinskis, K.C. and Povinelli, L.A., "Application of a Quasi-Three-Dimensional Inviscid Flow and Boundary Layer Analysis to the Hub-shroud Contouring of a Radial Turbine," AIAA Paper 84-1297, June 1984.

2. Anderson, D.A., Tannehill, J.C., and Pletcher, R.H., Computational Fluid Mechanics and Heat Transfer, Hemisphere Publishing Co., Washington, 1984.
3. Katsanis, T., "Calculation of Three-Dimensional Viscous Flow Through Turbomachinery Blade Passages by Parabolic Marching," AIAA Paper 85-1408, July 1985.
4. Denton, J.D., "A Time Marching Method for Two- and Three-Dimensional Blade to Blade Flow," ARC-R.&M.-3775, Aeronautical Research Council, London, 1975.
5. Denton, J.D. and Singh, U.K., "Time Marching Methods for Turbomachinery Flow Calculation," Application of Numerical Methods to Flow Calculations in Turbomachines, VKI-LEC-SER-1979-7, Von Karman Institute for Fluid Dynamics, Rhode-Saint-Genese, Belgium, 1979.
6. Denton, J.D., "An Improved Time Marching Method for Turbomachinery Flow Calculation," Journal of Engineering for Power, Vol. 105, No. 3, July 1983, pp. 514-524.
7. Denton, J.D., "A Method of Calculating Fully Three-Dimensional Inviscid Flow Through Any Type of Turbomachine Blade Row," Aerothermodynamics of Low Pressure Steam Turbines and Condensers, Vol. 1, VKI-LS-1983-06-VOL-1, Von Karman Institute for Fluid Dynamics, Rhode-Saint-Genese, Belgium, 1983.
8. Povinelli, L.A., "Assessment of Three-Dimensional Inviscid Codes and Loss Calculations for Turbine Aerodynamic Computations," Journal of Engineering for Gas Turbines and Power, Vol. 107, No. 2, Apr. 1985, pp. 265-276.
9. Goldman, L.J.; and Seasholtz, R.G., "Laser Anemometer Measurements in an Annular Cascade of Core Turbine Vanes and Comparison with Theory," NASA TP-2018, 1982.
10. Schwab, J.R., Stabe, R.G., and Whitney, W.J., "Analytical and Experimental Study of Flow Through an Axial Turbine Stage with a Nonuniform Inlet Radial Temperature Profile," AIAA Paper 83-1175, June 1983.
11. McLallin, K.L.; and Haas, J.E., "Experimental Performance and Analysis of 15.04-cm-tip-diameter, Radial-inflow Turbine with Work Factor of 1.126 and Thick Blading," NASA TP-1730, 1980.
12. Bosman, C.; and Highton, J., "A Calculation Procedure for Three-Dimensional, Time-Dependent, Inviscid, Compressible Flow Through Turbomachine Blades of Any Geometry," Journal of Mechanical Engineering Science, Vol. 21, No. 1, Feb. 1979, pp. 39-49.
13. Glassman, A.J.; and Wood, J.R., "Input Generator for Denton Three-Dimensional Turbomachine-Blade-Row Analysis Code," NASA TM-83324, 1983.

14. Katsanis, T.; and McNally, W.D., "Revised FORTRAN Program for Calculating Velocities and Streamlines on the Hub-Shroud Midchannel Stream Surface of an Axial-, Radial-, or Mixed-Flow Turbomachine or Annular Duct, I-User's Manual," NASA TN-D-8430, 1977.

TABLE I. - SUMMARY OF CORRECTED EXPERIMENTAL CONDITIONS (ref. 11)

Turbine-inlet total temperature, K	288.2
Turbine-inlet total pressure, N/m ²	101 300
Rotor-inlet to stator-inlet total pressure ratio	0.937
Rotor-inlet total pressure, N/m ²	94 918 (at station 3)
Rotative speed, rpm	31 456
Stator-inlet total pressure to rotor-exit static pressure ratio	3.255
Exit static pressure on the hub, N/m ²	31 120 (at station 4)
Mass-averaged absolute flow angle at rotor inlet, deg	73.6 (at station 3)
Mass flow rate, kg/s	0.2372

ORIGINAL PAGE IS
OF POOR QUALITY

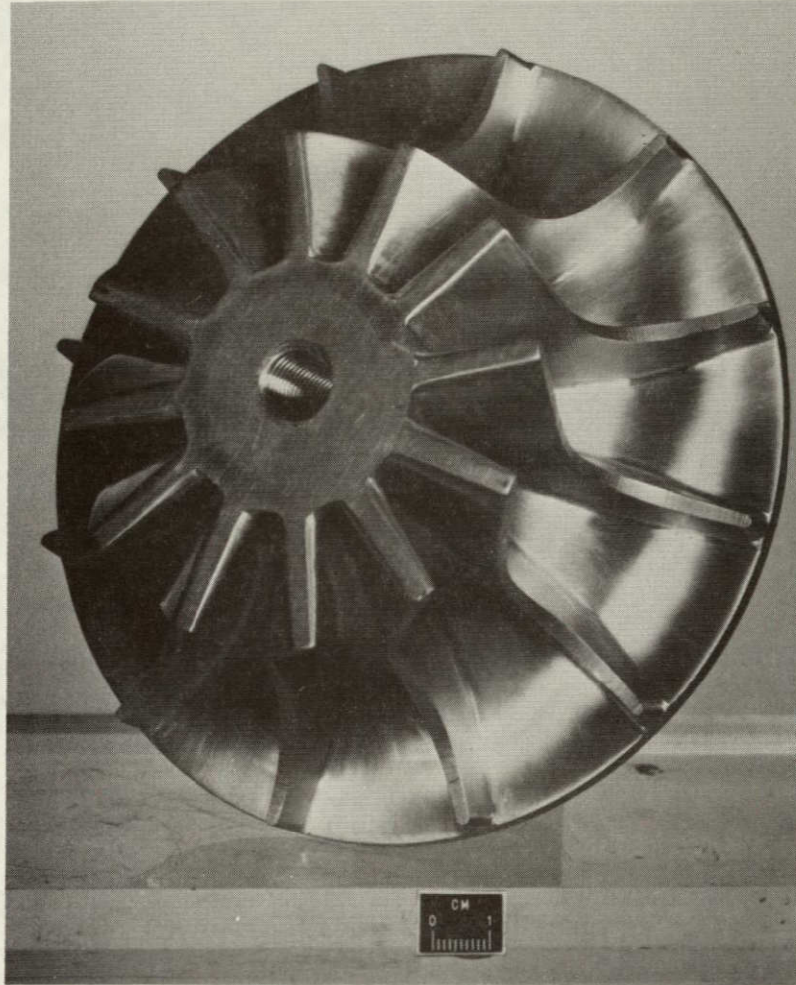


Figure 1. - Radial turbine rotor.

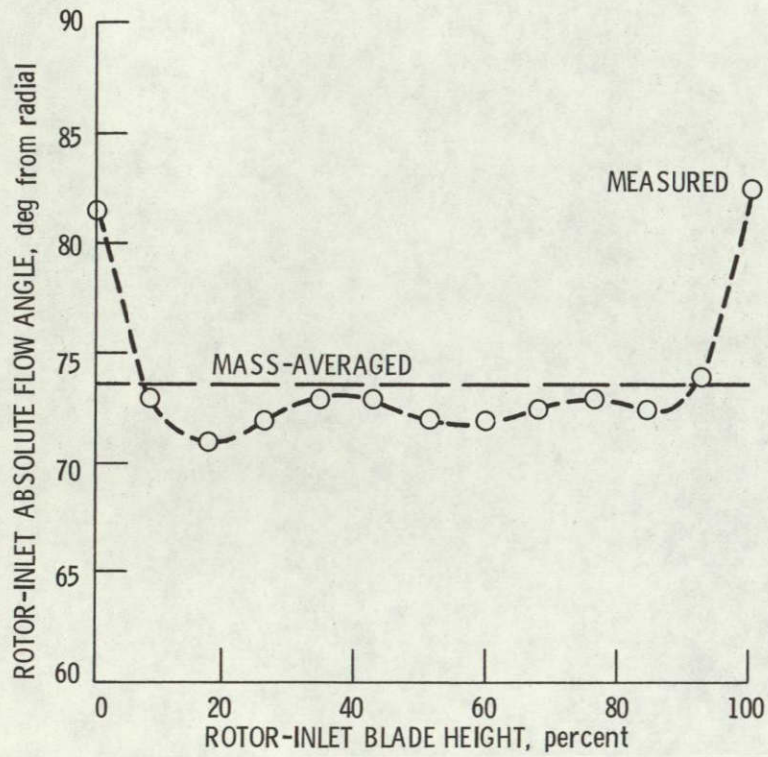


Figure 2. - Rotor-inlet absolute flow angle.

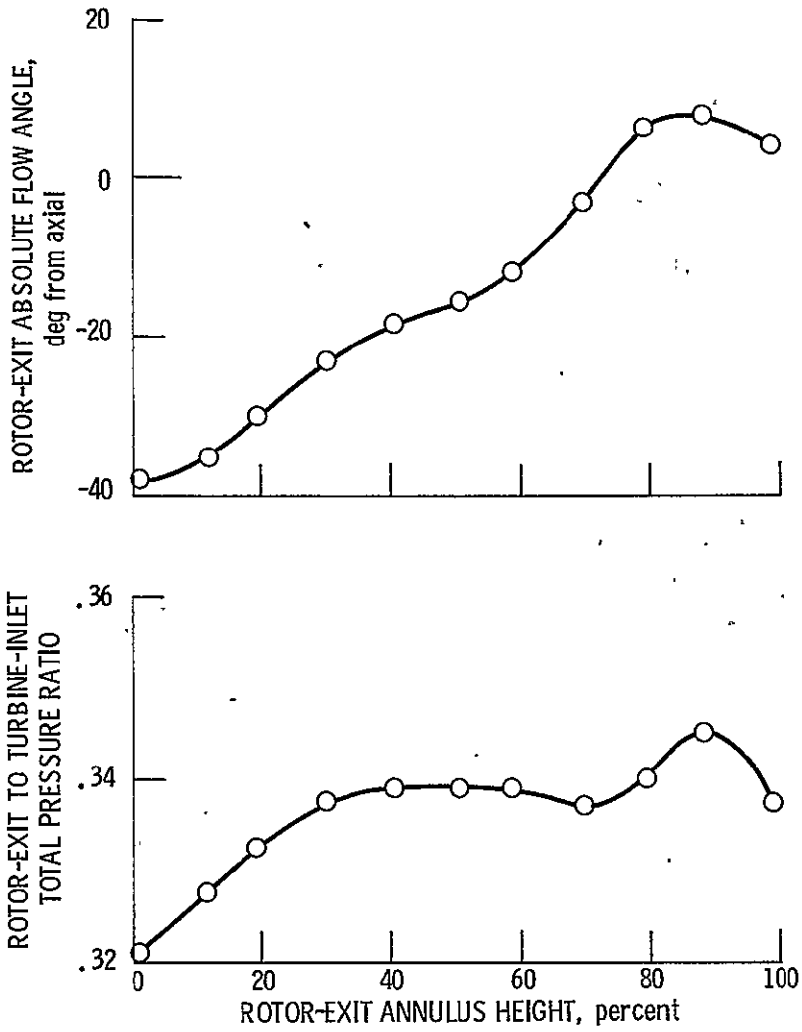


Figure 3. - Measured data at rotor exit.

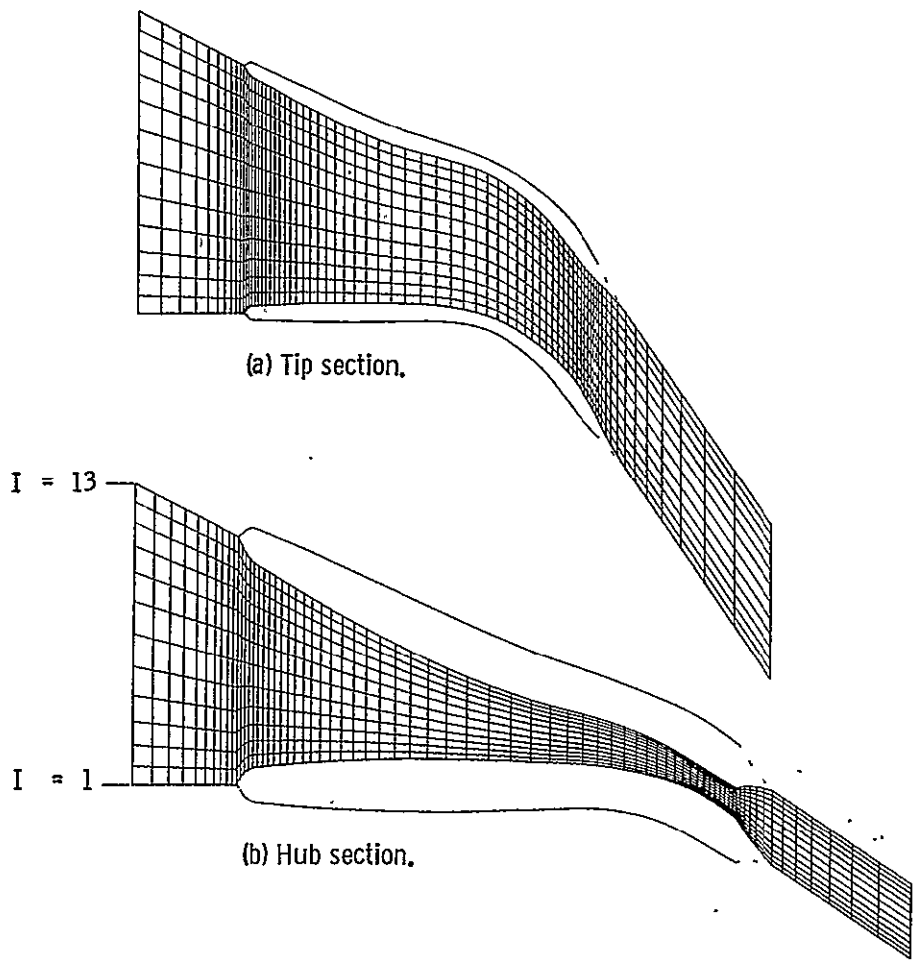


Figure 4. - Computational mesh on blade-to-blade surfaces.

ORIGINAL PAGE IS
OF POOR QUALITY

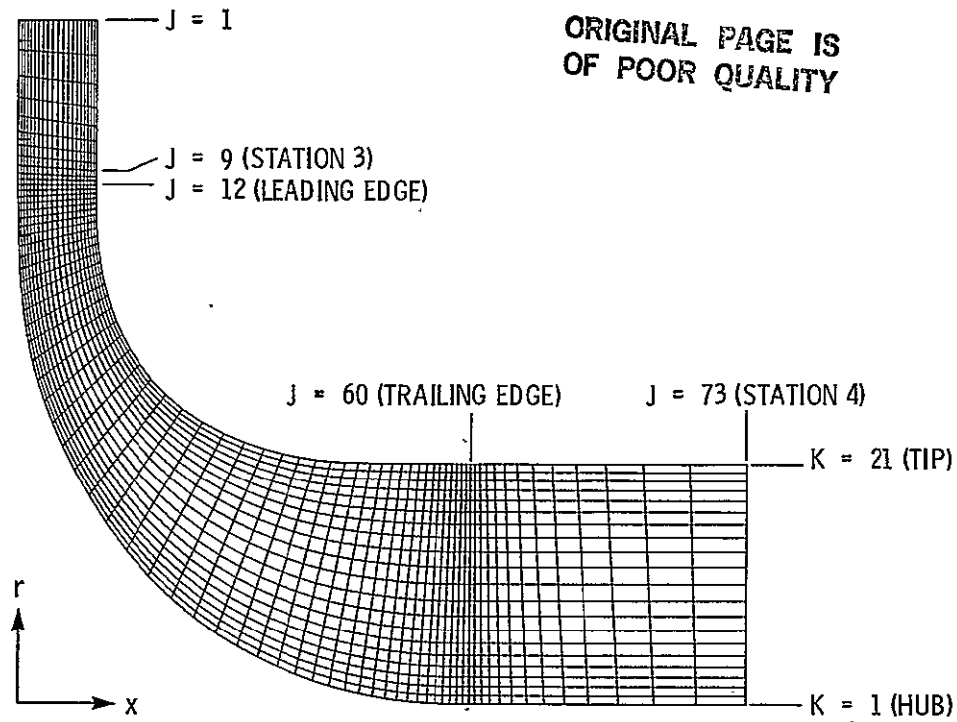


Figure 5. - Computational mesh in meridional plane.

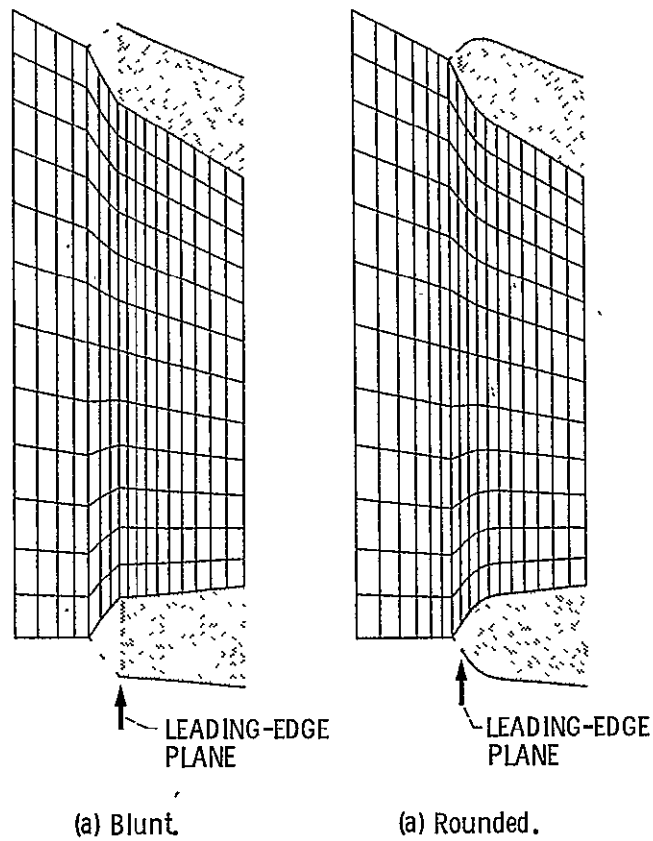


Figure 6. - Leading-edge cusps.

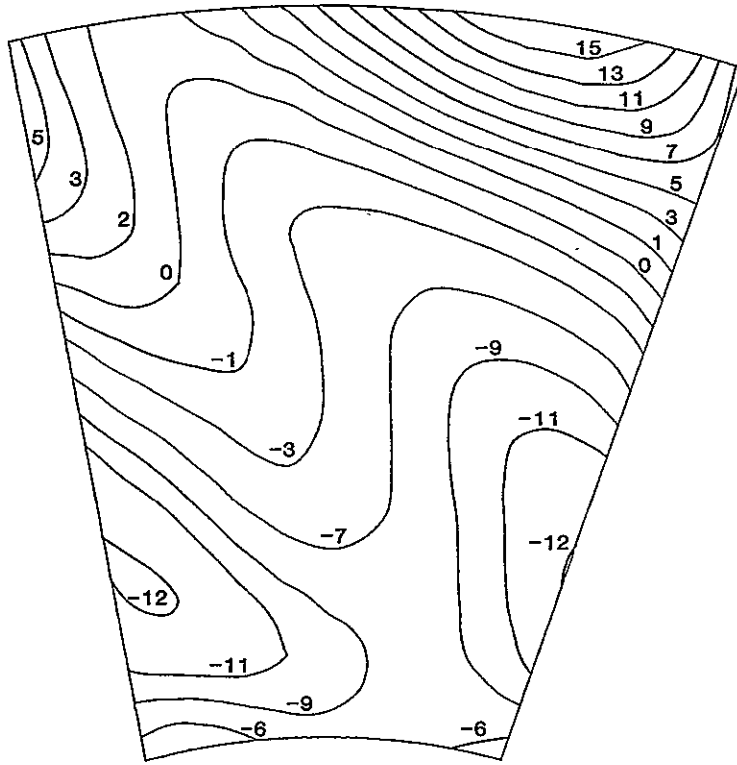
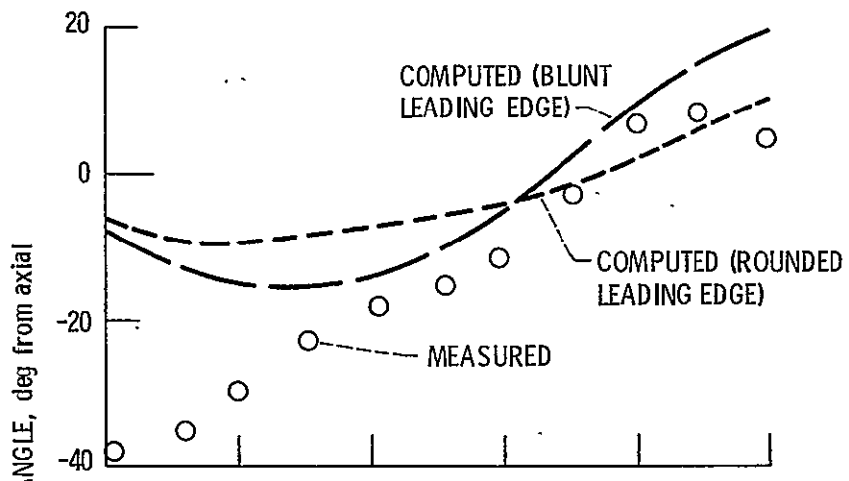
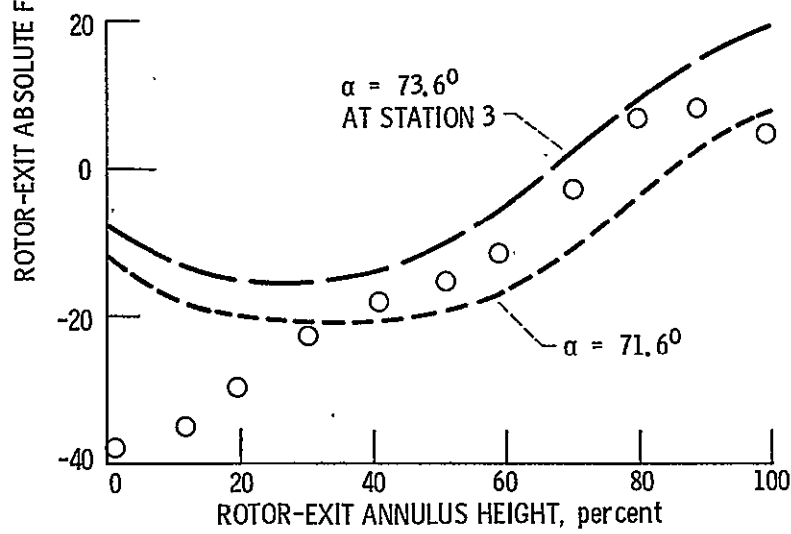


Figure 7. - Absolute flow angle contour map at station 4, degrees from axial.



(a) Measured vs computed results.



(b) Effect of rotor-inlet absolute flow angle on the exit absolute flow angle.

Figure 8. - Rotor-exit absolute flow angle.

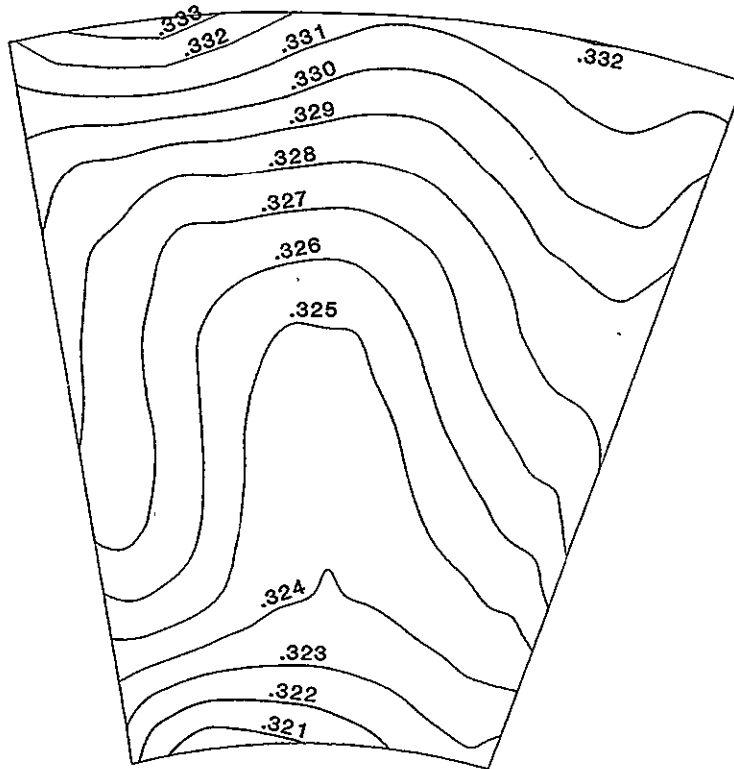
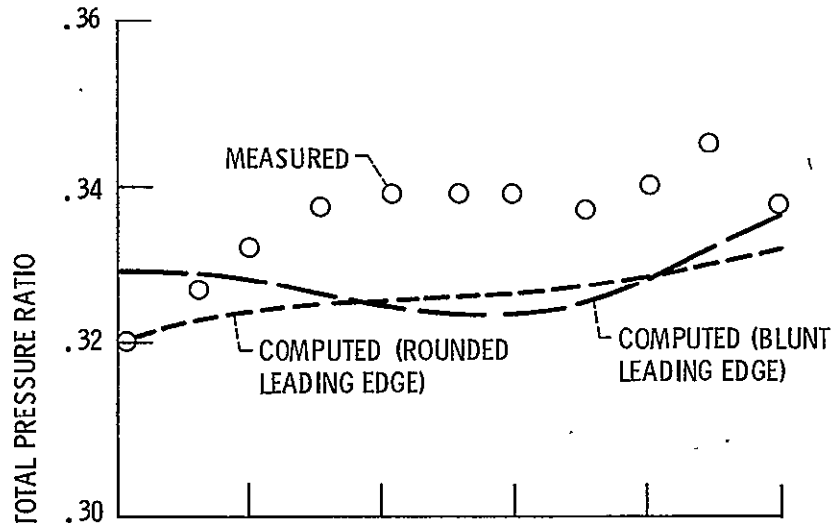
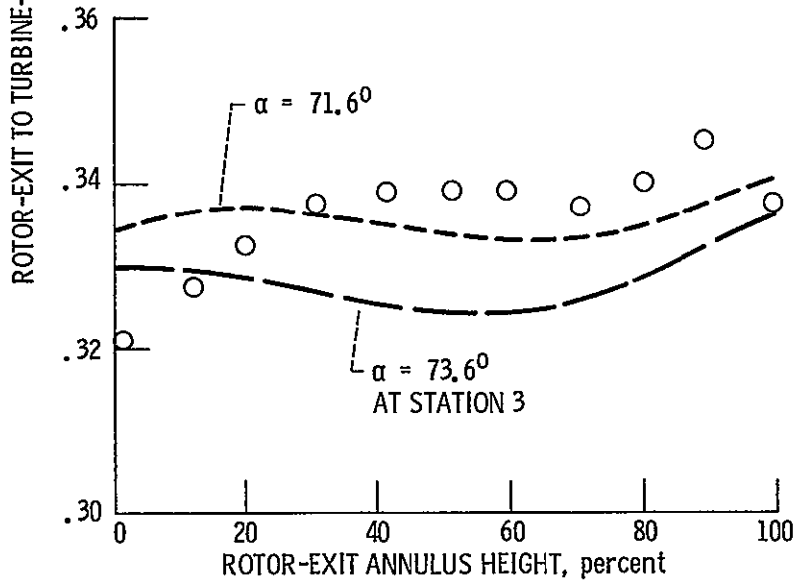


Figure 9. - Distribution of the rotor-exit to turbine-inlet total pressure ratios on the cross-channel surface at station 4.



(a) Measured vs computed results.

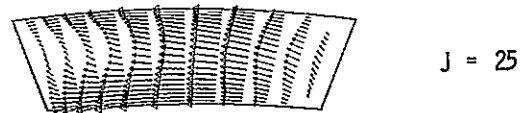
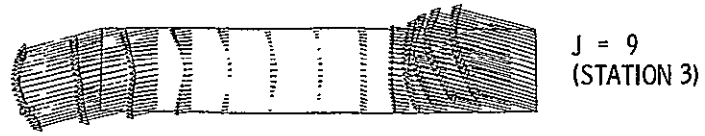


(b) Effects of rotor-inlet absolute flow angle on the total pressure ratio.

Figure 10. - Rotor-exit to turbine-inlet total pressure ratio.

$0.25 W_m$
→
 W_m : AVERAGE MERIDIONAL VELOCITY

ORIGINAL PAGE IS
OF POOR QUALITY



PRESSURE

SUCTION

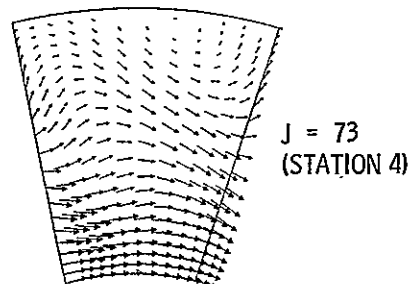
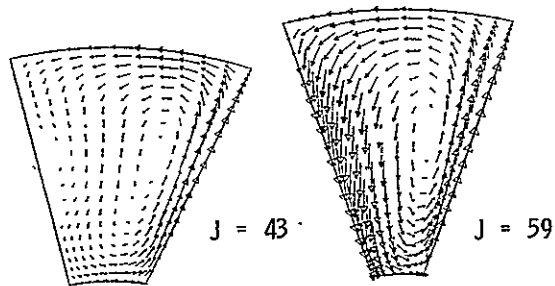
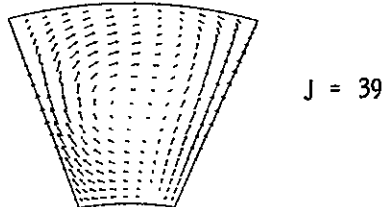
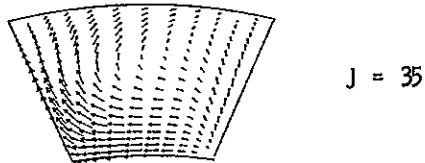


Figure 11. - Evolution of a passage vortex.

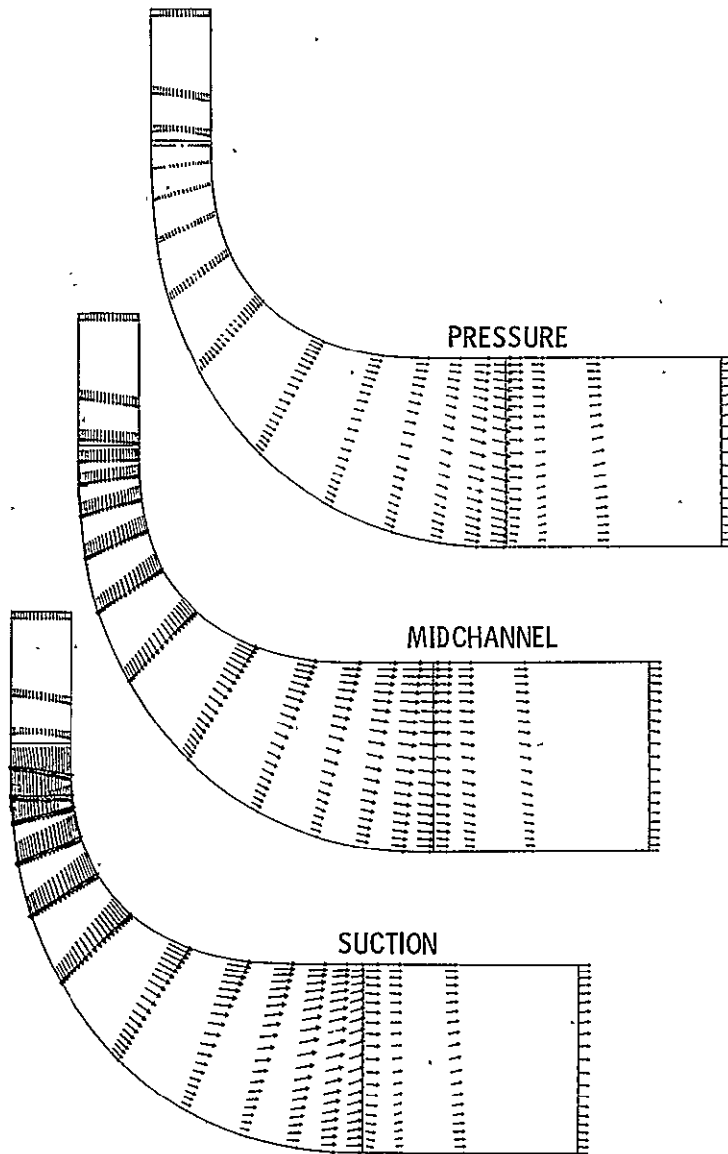
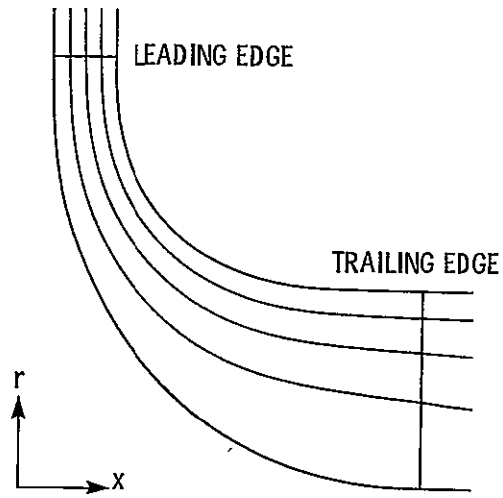
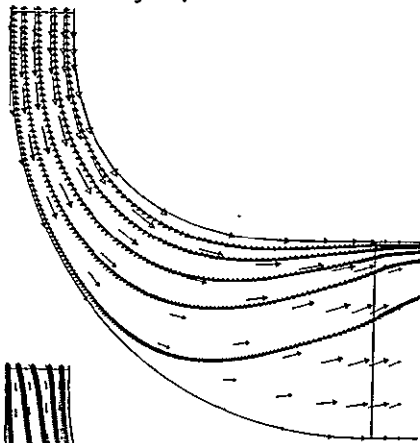


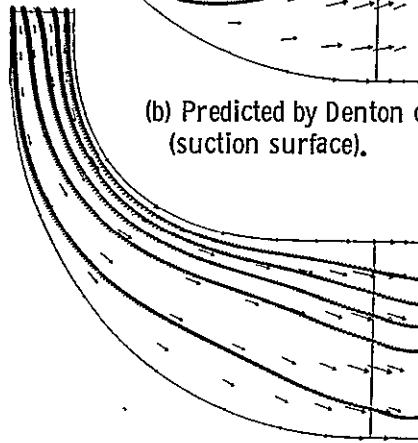
Figure 12. - Velocity components on meridional planes.



(a) Predicted by a quasi-three-dimensional analysis.



(b) Predicted by Denton code (suction surface).



(c) Predicted by Denton code (pressure surface).

Figure 13. - Meridional streamlines.

ORIGINAL PAGE IS
OF POOR QUALITY

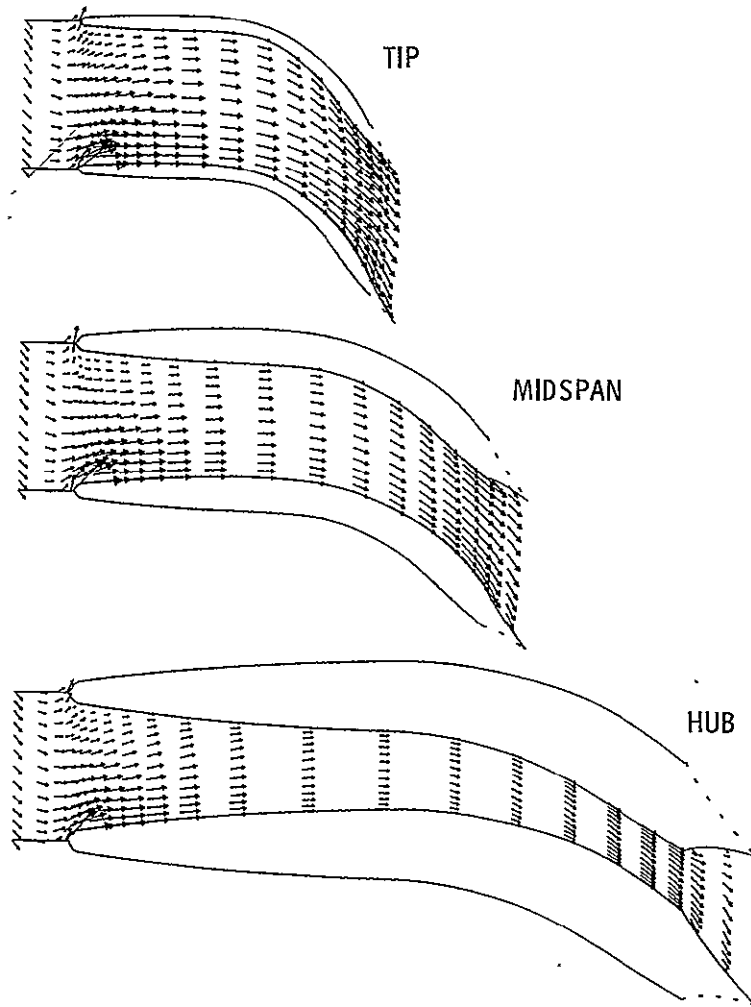


Figure 14. - Velocity components on blade-to-blade surfaces.

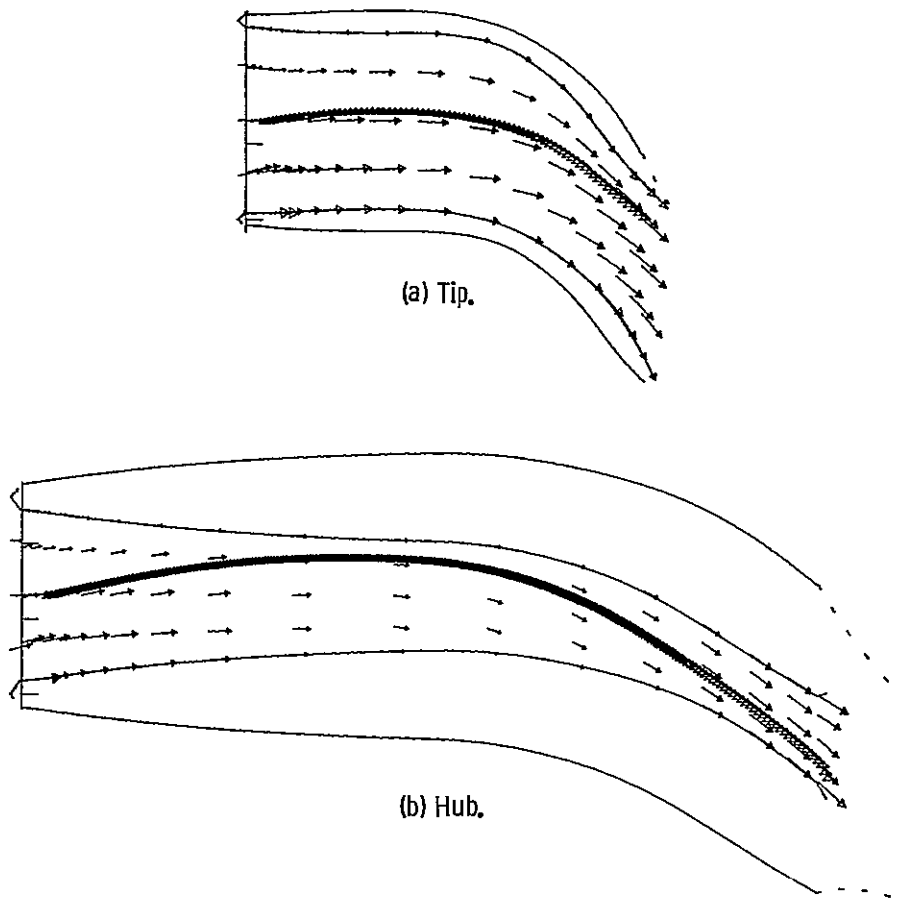


Figure 15. - Streamlines predicted by the Denton code.

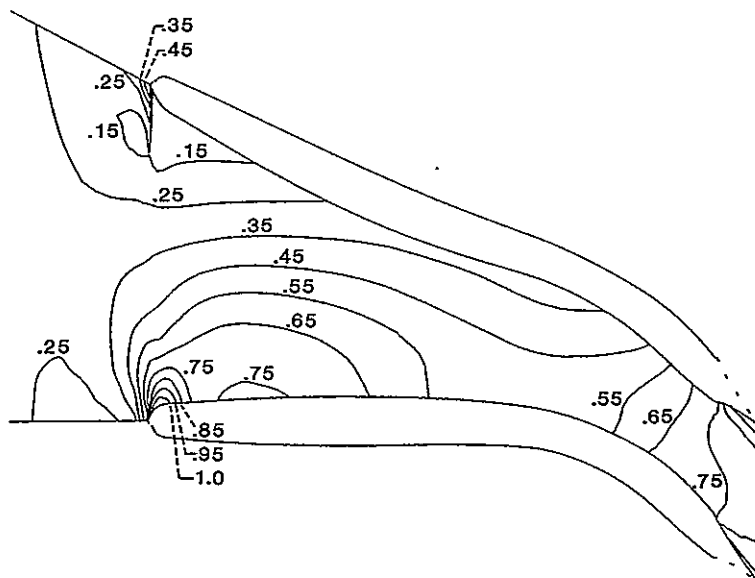
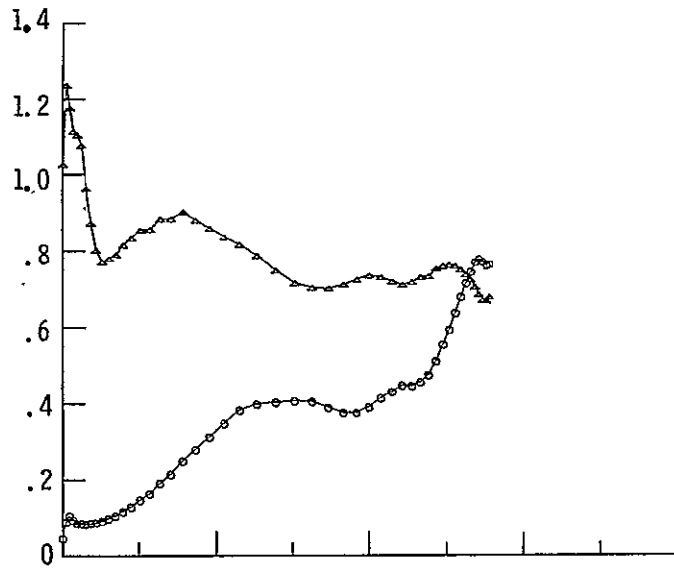
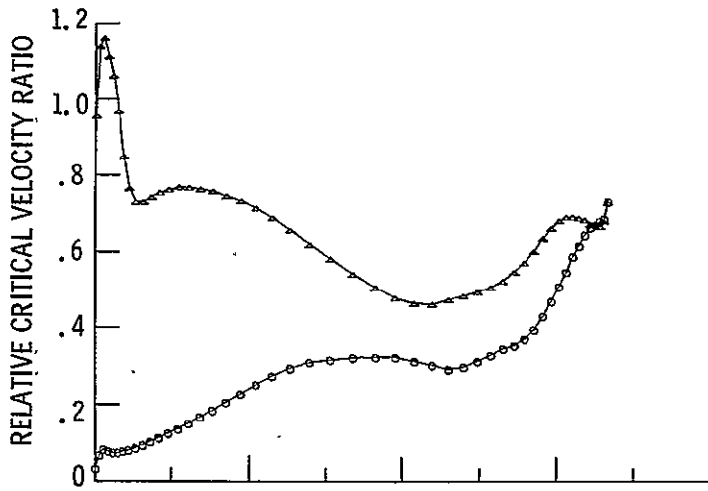


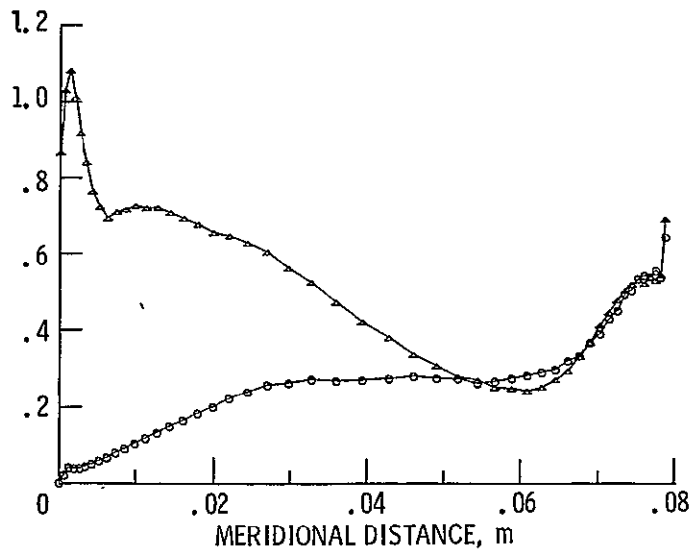
Figure 16. - Relative critical velocity ratios on the midspan blade-to-blade surface.



(a) Tip.



(b) Midspan.



(c) Hub.

Figure 17. - Blade-loading diagram.

1. Report No. NASA TM-87091 USAAVSCOM-TR-85-C-12		2 Government Accession No.		3 Recipient's Catalog No.	
4. Title and Subtitle Three-Dimensional Inviscid Analysis of Radial Turbine Flow and a Limited Comparison with Experimental Data				5. Report Date	
				6 Performing Organization Code 505-31-04	
7. Author(s) Y.K. Choo and K.C. Civinskas				8 Performing Organization Report No. E-2679	
				10. Work Unit No.	
9. Performing Organization Name and Address NASA Lewis Research Center and Propulsion Directorate U.S. Army Aviation Research and Technology Activity (AVSCOM), Cleveland, Ohio 44135				11. Contract or Grant No.	
				13. Type of Report and Period Covered Technical Memorandum	
12 Sponsoring Agency Name and Address National Aeronautics and Space Administration Washington, D.C. 20546 and U.S. Army Aviation Systems Command, St. Louis, Mo. 63120				14. Sponsoring Agency Code	
15. Supplementary Notes Y.K. Choo, NASA Lewis Research Center; K.C. Civinskas, Propulsion Directorate, U.S. Army Aviation Research and Technology Activity (AVSCOM). Prepared for the Three-Dimensional Flow Phenomena in Fluid Machinery Symposium, ASME Winter Annual Meeting, Miami, Florida, November 17-22, 1985.					
16. Abstract The three-dimensional inviscid DENTON code was used to analyze flow through a radial-inflow turbine rotor. Experimental data from the rotor are compared with analytical results obtained by using the code. The experimental data available for comparison are the radial distributions of circumferentially averaged values of absolute flow angle and total pressure downstream of the rotor exit. The computed rotor-exit flow angles are generally underturned relative to the experimental values, which reflect the boundary-layer separation at the trailing edge and the development of wakes downstream of the rotor. The experimental rotor was designed for a higher-than-optimum work factor of 1.126 resulting in a nonoptimum positive incidence and causing a region of rapid flow adjustment and large velocity gradients. For this experimental rotor, the computed radial distribution of rotor-exit to turbine-inlet total pressure ratios are underpredicted due to the errors in the finite-difference approximations in the regions of rapid flow adjustment and due to using the relatively coarser grids in the middle of the blade region where the flow passage is highly three-dimensional. Additional results obtained from the three-dimensional inviscid computation are also presented, but without comparison due to the lack of experimental data. These include quasi-secondary velocity vectors on cross-channel surfaces, velocity components on the meridional and blade-to-blade surfaces, and blade surface loading diagrams. Computed results show the evolution of a passage vortex and large streamline deviations from the computational streamwise grid lines. Experience gained from applying the code to a radial turbine geometry is also discussed.					
17. Key Words (Suggested by Author(s)) Turbines; Three-dimensional flow; Radial flow; Inviscid flow; Aerodynamics				18. Distribution Statement Unclassified - unlimited STAR Category 02	
19. Security Classif. (of this report) Unclassified		20. Security Classif. (of this page) Unclassified		21. No. of pages	22 Price*

National Aeronautics and
Space Administration

Lewis Research Center
Cleveland, Ohio 44135

Official Business
Penalty for Private Use \$300

SECOND CLASS MAIL

ADDRESS CORRECTION REQUESTED



Postage and Fees Paid
National Aeronautics and
Space Administration
NASA-451

NASA
